1   **A database of radiogenic Sr-Nd isotopes at the "three poles"**

2   Zhiheng Du[a], Jiao Yang[a], Lei Wang[b], Ninglian Wang[c], Anders Svensson[d], Zhen

3   Zhang[e], Xiangyu Ma[f], Yaping Liu[a], Shimeng Wang[a], Jianzhong Xu[a], Cunde Xiao[b*]

4   [a]State Key Laboratory of Cryospheric Science, Northwest Institute of

5   Eco-Environment and Resources, Chinese Academy of Sciences, Lanzhou 730000,

6   China

7   [b]State Key Laboratory of Earth Surface Processes and Resource Ecology, Beijing

8   Normal University, Beijing 100875, China

9   [c]College of Urban and Environmental Sciences, Northwest University, Xi'an 710127,

10   China

11   [d]Centre for Ice and Climate, Niels Bohr Institute, University of Copenhagen,

12   Copenhagen, Denmark

13   [e]School of Spatial Informatics and Geomatics Engineering, Anhui University of

14   Science and Technology, Huainan 232001, China

15   [f]Qingdao Blue Thinking Information Technology Co.Ltd, Qinggao 266555, China

16   *Correspondence and requests for materials should be addressed to CD. X

17   (cdxiao@bnu.edu.cn).

19   **Abstract:** The radiogenic isotope compositions of strontium (Sr) and neodymium (Nd)

20   on the surface of the Earth are powerful tools for tracing dust sources and sinks on

21   Earth's surface. To differentiate between the spatial variabilities of aeolian dust

22   sources in key cryospheric regions at the three poles (including the 'Third Pole'

23   covering the high mountainous area in Asia, the Arctic and Antarctica), a dataset of

24   the Sr-Nd isotopic compositions from the terrestrial extremely cold or arid

25   environments in this study was compiled, similar to the method of Blanchet (2019).

The database identified snow, ice, sand, soil (loess), sediment, and rock from the modern and Quaternary periods of the three poles based on 90 different references and our own measurement data, with a total of 1989 data points, 206 data points with different grain sizes and 209 data points with fraction measurements. There are 485 data points from the Third Pole, 727 data points from the Arctic, and 777 data points from the Antarctica. The sampling and measurement methods of these data are introduced. For each pole, geographical coordinates and other information are provided. The main scientific purpose of this dataset is to provide collective documentation and our own measurements for the Sr-Nd dataset, which will be useful for determining the sources and transport pathways of dust in snow and ice, river, and oceans at the three poles, and to investigate whether multiple dust sources are present at each of the poles. This dataset provides exhaustive detailed documentation of the isotopic signatures at the three poles during specific time intervals of the Quaternary period, which are useful for understanding the sources or sinks of aeolian dust or sediments at the three poles. The datasets are available from the National Tibetan Plateau Data Center (https://doi.org/10.11888/Cryos.tpdc.272100, Du et al., 2022).

Keywords: Radiogenic isotopic dataset, Third Pole, Arctic Ocean, Southern Ocean, Greenland and Antarctic ice sheets, Dust provenances.

1. Introduction

The role of mineral dust in the Earth system extends well beyond its impact on the energy balance and involves interactions with the carbon cycle and glacier melting on global scales (Skiles et al., 2018; Shao et al., 2011). The transport of dust from the low mid-latitudes, which contain major deserts that are dust sources, to the Arctic region or AIS is sensitive to amplified high-latitude climatic variability (Bory et al., 2003a; Bory et al., 2003b; Lupker et al., 2010; Lambert et al., 2013: Struve et al.,

2020). The isotopic compositions of the radiogenic isotopes strontium (Sr) and neodymium (Nd) are powerful tools for tracing dust sources and sinks because their characteristics are significantly different on the surface of the Earth (including snow, sand, sediment, loess and aeolian deposits) (Grousset et al., 2005; Chen et al., 2007; Xu et al., 2012; Robinson et al., 2021). Therefore, the combination of different isotopic signatures, specifically $^{87}Sr/^{86}Sr$ and $^{143}Nd/^{144}Nd$ (expressed as $\varepsilon_{Nd}(0)$), has proven to be useful in discriminating different dust source areas in Earth science.

The transport of aeolian dust from natural desert regions has also been identified in modern snow and ice records at the third pole based on Sr-Nd data (Wu et al., 2010; Xu et al., 2012; Du et al., 2015; Dong et al., 2018). Many studies have focused on dust transport from the western Chinese deserts to the Chinese loess plateau (CLP), Pacific Ocean and even the Greenland ice sheet (GrIS) (Biscaye et al., 1997; Chen et al., 2007; Wei et al., 2021). However, it is still a controversial issue; for example, recent results have emphasized that aeolian dust from local sources contributes significantly to high mountain glaciers (Du et al., 2019a; Wei et al., 2021). And aeolian dust from various source regions, including the Saharan Desert in North Africa and the Gobi and Taklimakan Deserts in Asia, is transported to the Greenland snow and ice, and there are still great uncertainties (Han et al., 2018).

The Sr-Nd data in snow layers at the Berkner Island ice sheet in western Antarctica, for most of the year, are data support scenarios that involve contributions from proximal sources (Bory et al., 2010). The Sr-Nd data from insoluble dust in snow samples from East Antarctica indicate that long-distance natural dust primarily originates from Australia and that local dust originates from ice-free areas (Du et al., 2018). The Sr-Nd data in the Taylor Glacier zero-age ice samples and snow samples from Roosevelt Island could be a mixture of at least two local sources (Winton et al.,

2016; Aarons et al., 2017). The Sr-Nd data from East Antarctica ice cores during the Holocene indicate a well-mixed atmospheric background involving a mixture of two or more sources in the Southern Hemisphere (SH) (Aarons et al., 2016, 2017; Delmonte et al., 2019). The amount of isotopic information is currently adequate for Patagonian and non-Patagonian mineral dust exported from southern South America and the East Antarctic ice sheet (EAIS) (Grousset et al., 1992; Gaiero et al., 2007; Delmonte et al., 2010a, b, 2019; Delmonte et al., 2013; Blakowski et al., 2016; Aarons et al., 2017). Major efforts have attempted to solve the 'puzzle' of the origin of the potential source areas that contribute dust to the Southern Ocean (SO) and the whole Antarctic Ice Sheet (AIS) (Gili et al., 2021). However, Sr-Nd data in the entire AIS have an uneven distribution. Measuring Sr-Nd stable isotopic compositions in ice cores from Antarctica is a major challenge.

As much Sr-Nd data were measured, these data characteristics and measurement methods, which is necessary to reassess these data on the dust sources in these remote regions. Therefore, the amounts of Sr-Nd data measured in snow, soil, sediment, sand and other samples should be integrated into a dataset to better serve the environmental and climatic sciences studying the third regions in the future. The answers to these questions have been hindered by a paucity of Sr-Nd data, which provide information on the local and potential dust sources. For these reasons, we measured Sr-Nd data in some samples and collected Sr-Nd data in the literature at the three poles (Fig. 1, Table 1). Therefore, the objective of this work was to produce a compilation of published and unpublished data from the three poles, and the specific time intervals of Sr-Nd data were limited to the Quaternary period. As an example, the modern dust (Holocene) in snow or ice and sediment sample contributions from the three poles were further discussed, and the potential dust transport paths in Greenland and

Antarctic ice sheets were traced. Similar to the method of Blanchet (2019), here, we compile published and unpublished Sr-Nd data with an integrated filtering system from three remote poles, in which these data were collected in extremely cold or arid environments, and most of the data were not included in the previous dataset. The dataset will help trace modern natural dust, reconstruct past environments, and extend the database of terrestrial and marine radiogenic Sr and Nd isotope data in the Earth and environmental sciences.

2. Sample measurement and data processing

2.1 Sample collection and measurement

Sr-Nd data in snow, sand, soil, cryoconite, loess and sediment samples were collected from our own research and literature from three poles (the 'Third Pole' covering the high mountainous area in Asia, the Arctic and Antarctica) (Fig. 1). Sr-Nd data in the Third Pole cover the area of $40°$ to $23°N$ and $106°$ to $61°E$ and included data from arid deserts and mountains in northern China (Fig. 2). Sr-Nd data in the Arctic from the high Arctic to the sub-Arctic areas, and Sr-Nd data in Antarctica refer to the area including the entire Antarctic continent, the AIS, and the Antarctic Peninsula (>$60°S$). Sr-Nd data were collected from Australia, southern South America (SSA), southern Africa (SA) and New Zealand (Fig. 1). The cryoconite samples indicate that the mixtures and/or aggregates of these biotic and abiotic impurities on glacial ice, were collected at different elevations in glaciers (Table 2). Note that the Sr-Nd data from the snow, ice core, surface aeolian dust, deposit samples, and the ages of these samples are almost all less than one million. Therefore, the ages of Sr-Nd data are limited to the Quaternary period in this dataset.

126

127
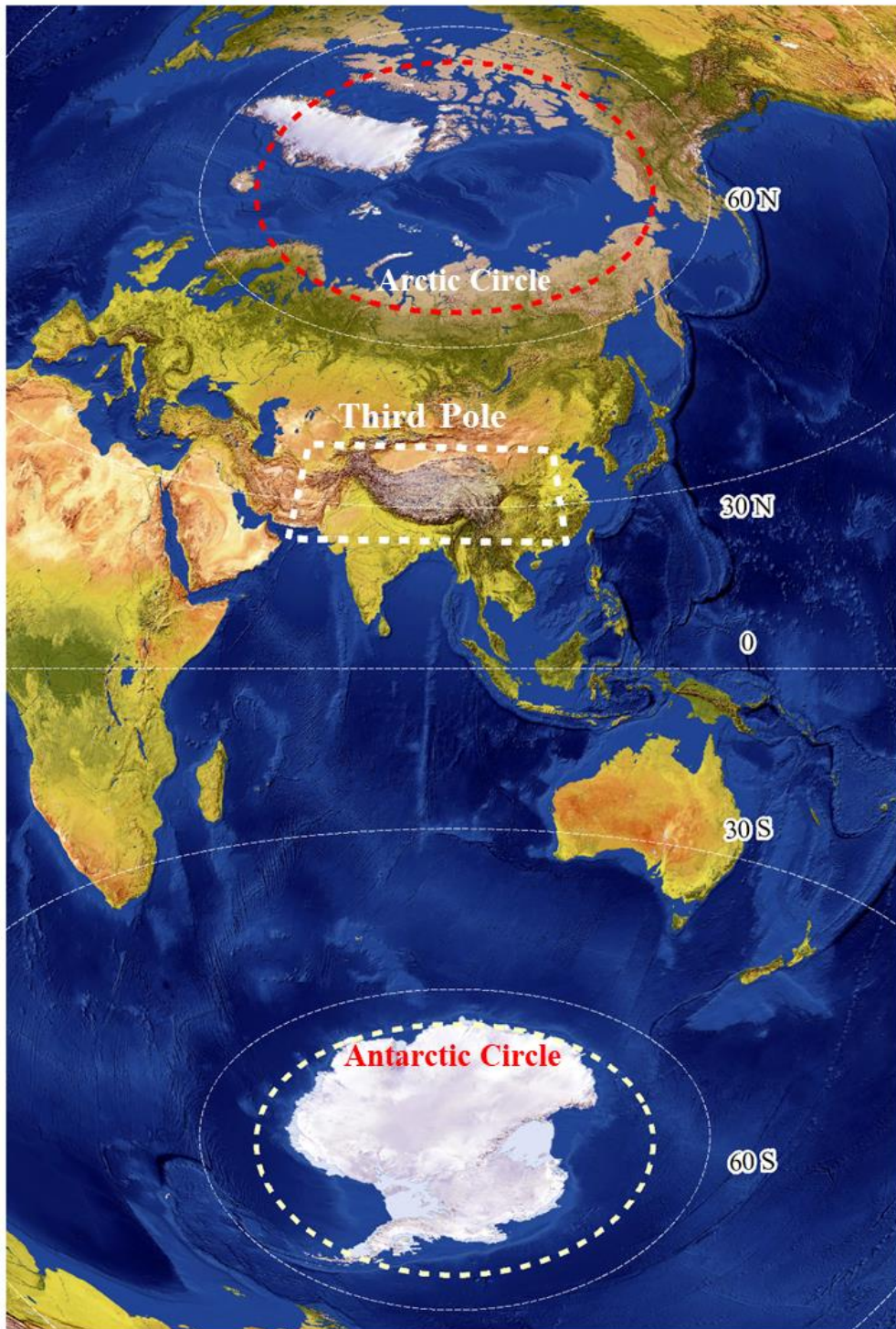
Fig. 1. Map of the sampling regions in the three poles (Third Pole: data were collected in the area of 40 ° to 23 °N and 106 ° to 61 °E, Li et al., 2020; Arctic: from the high Arctic to the sub-Arctic areas, data were collected >60 °N in this region); and

Antarctica: data were collected >60 ℃S in this region, which are indicated with different coloured circles) in this study (The background of this figure is from ArcGIS).

Two sand samples from Kangerlussuaq, West Greenland were collected. Four sand samples collected on King George Island and eleven sand samples collected on Inexpressible Island in the Ross Sea, West Antarctica, were measured in this study. In general, the upper 2 or 5 cm of surface topsoil (sand) was collected with a trowel and stored in precleaned plastic bags or bottles. The sediment samples from shelves and ridges in the Arctic Ocean (AO), which were mostly retrieved from core archives, were subsampled in the upper surface of the core tops (with rare exceptions) (Maccali et al., 2018). Different grain sizes (<5 μm, <10 μm, 30 μm, <63 μm, <75 μm and <100 μm fractions and bulk) of surface soil or sand were extracted by the sieving method (Chen et al., 2007; Maccali et al., 2018; Du et al., 2018, 2019a, b; Wei et al., 2021).

Snow samples were collected from the snowpit at a vertical resolution of 5–20 cm, following the clean-hands protocol with sampling personnel wearing integral Tyvek® bodysuits, nonpowdered gloves and masks to avoid possible contamination (Xu et al., 2012). In this study, one 1.0 m snowpit with a resolution of 10 cm was dug in the East Greenland ice sheet (GrIS), and four fresh snow samples (M1, M2, M3 and M4) were sampled on sea ice in the Arctic Ocean (AO) during fulfil mission of the Multidisciplinary drifting Observatory for the Study of Arctic Climate (MOSAIC) in October 2020. Surface fresh snow (2-10 cm) samples at different resolutions (with different thicknesses, widths and lengths) in Greenland and Antarctica ice sheets were excavated and placed in 5 L Whirl-Pak bags (Du et al., 2018; Du et al., 2019a, b). Three horizontal snow layers were collected for Greenland and Antarctica snowpits (Bory et al., 2003b; Bory et al., 2010). The dust in the ice core was extracted using the

same method as that for the snow samples. Snow or ice core samples are nearly bulk samples or have different grain sizes (>0.2 μm, > 0.45 μm, > 0.45 μm and <30 μm) (Du et al., 2015, 2019b; Bory et al., 2003 a, b; Bory et al., 2010; Lupker et al., 2010; Wu et al., 2010).

2.2 Data processing

Sr-Nd isotope datasets from snow, ice cores, sand, sediment, soil and loess samples from the Third Pole, Arctic and Antarctica were compiled. Data were collected from 90 different references with 2844 data points. In total, 485 data points were collected from the Third Pole, 727 data points were collected from the Arctic, and 777 data points were collected from the Antarctica. In addition, 259 data points were collected from the Pan-third pole, and 181 data points were included from the potential source areas (PSAs) of SH. Details of geographical coordinates and original information can be found in this dataset, and the locations of these samples are shown on maps. To keep the naming scheme uniform, the dataset assembled the names of each sample based on the work by Blanchet (2019). This dataset was built by incorporating data from the literature and our own database; in particular, units, source or sink and geographical coordinates are marked in the dataset. Note that the Sr-Nd data whether represent source or sink information, which need determine based on the detail depositional environment or distribution. For examples, the loess samples from the CLP represent the sink, which it also represent the dust source for the Pacific Ocean. Therefore, these samples were marked with mixture. And the sediment samples from the coast of SO or AO (Rivers or Dune sand) were also marked with mixture. An overview of the input data is shown in Table 1. The study focuses on the large amounts of different data, including data on snow, ice, sand, soil, loess, sediment, etc. The data are based on our own measurements, author

181 contributions (data published) and literature searches.

182 All subsequent procedures were performed in clean lab facilities. The sand, loess,

183 sediment, cryoconite and dust extracted from snow or ice cores were generally

184 digested with ultrapure acid (HNO_3, HF and $HClO_4$ or HNO_3, HF and HCl), and

185 $^{87}Sr/^{86}Sr$ and $^{143}Nd/^{144}Nd$ ratios were determined by the different types of

186 thermoionization mass spectrometry or multiple collector inductively coupled

187 plasma-mass spectrometry. Sr-Nd values, with uncertainties expressed as $\pm2\sigma\times10^{-6}$ (2

188 standard errors of the mean), can also be found in the original references. The

189 $^{143}Nd/^{144}Nd$ isotopic composition is expressed as:

190 $\varepsilon_{Nd}(0) = ((^{143}Nd/^{144}Nd)_{Sample}/(^{143}Nd/^{144}Nd)_{CHUR}-1)\times10^4$, where $(^{143}Nd/^{144}Nd)_{CHUR}$

191 $= 0.512638$, where CHUR stands for chondritic uniform reservoir and represents a

192 present-day average Earth value $(^{143}Nd/^{144}Nd)_{CHUR}=0.512638$ (Jacobsen &

193 Wasserburg 1980).

194 **3. Data descriptions**

195 **3.1. Reliability assessment for the differences in Sr-Nd based on grain sizes,**

196 **lithogenic and measuring methods**

197 The grain size effect in different samples resulted in $^{87}Sr/^{86}Sr$ ratio and $\varepsilon_{Nd}(0)$

198 variations. For surface aeolian sand and marine sediment samples, the variations in

199 size-separated $^{87}Sr/^{86}Sr$ values are slightly affected by grain size (Chen et al., 2007;

200 Tütken et al., 2002). The Sr isotope ratios in loess from the CLP tended to be higher in

201 the fine fraction and were much higher in the <2 μm fraction than in other coarser

202 fractions (Rao et al., 2006). However, the variations in the $^{87}Sr/^{86}Sr$ isotopic ratios in

203 alpine soils of the Tibetan Plateau are not clearly related to the carbonate effect and

204 grain size effect (Lin and Feng, 2015). $\varepsilon_{Nd}(0)$ values clearly exhibits the grain

205 size-dependent variability, because $\varepsilon_{Nd}(0)$ values seem not to be fractionated between

mineralogically different grain-size fractions during the sedimentary cycle (Tüken et al., 2002; Xie et al., 2020). While a substantial proportion of Sr-Nd isotope values showed enrichment in the coarse-grained fraction (< 63 μm, 30-63 μm, 10–30 μm and < 10 μm) (Xie et al., 2020). Within the isotopically diverse Indus delta sediment, bulk isotopic compositions are estimated to deviate on average no than ±1.04 ε_{Nd} units and ±0.0099 for $^{87}Sr/^{86}Sr$ values for any sediment as a result of mineralogy, grain size distribution, and analytical error (Jonell et al., 2018)..

The $\varepsilon_{Nd}(0)$ signatures of the lithic fraction of the sediments are taken as a robust circulation and hydrologic proxies applicable because of its different origins across timescales (Revel et al., 1996; Abbott et al., 2022). However, Sr-Nd isotope ratios in the lithogenic sediment fraction represent a complex mixture (Meinhardt et al., 2016; Bayon et al., 2021). The widespread influence of lithogenically sourced neodymium on authigenic $\varepsilon_{Nd}(0)$ had been demonstrated. Such as, there is a strong linear relationship between detrital $\varepsilon_{Nd}(0)$ and authigenic $\varepsilon_{Nd}(0)$ (r=0.86, n=871). Therefore, the sediment characteristics and detrital isotope records should be considered when used $\varepsilon_{Nd}(0)$ data (Abbott et al., 2022). The different acid leaching methods also have an effect on the Sr-Nd isotopic composition in the silt and clay fractions in marine sediments (Walter et al., 2000). Loess samples from the CLP and cryoconites (including surface dust) from high mountain glaciers had obviously higher $^{87}Sr/^{86}Sr$ ratios after acid treatment than before (Rao et al., 2016; Nagatsuka et al., 2010, Nagatsuka et al., 2019). In addition, $\varepsilon_{Nd}(0)$ of the leachable in the surface sediment samples implied the North Atlantic deep water circulation pattern. Sr-Nd data in Fe–Mn fractions of marine sediments can be used in paleoceanography to infer transportation of terrigenous material and changes in bottom-water circulation (Bayon et al., 2002; Asahara et al., 2012).

231   Therefore, assuming that Sr-Nd data in different media in this dataset were used

232   for interpreting Sr-Nd isotope compositions in terms of provenance and

233   paleoceanography, the grain sizes, lithogenic and measurement methods on these

234   isotopic data must be considered for better illustration using these data.

235   **3.2 The Sr-Nd data characteristics of glaciers at the Third Pole**

236   Table 2 and Fig. 2 provide an overview of the information (the serial number of

237   glaciers; sub-regions; glacier name; name of the sampling site where the samples were

238   taken; sample type, age, elevation; longitude and latitude and elevation) from the

239   Third Pole. The dust in snow or ice in the Third Pole absolutely originates from PSAs,

240   therefore, Sr-Nd data in these samples represents the characteristics of sinks. And

241   Sr-Nd data from the local or arid deserts sand or soil represents the characteristics of

242   PSAs. As an example, the isotopic signatures in insoluble dust of these snow/ice

243   (sinks) from the Third Pole can be traced that which originate from the possible PSAs

244   based on those Sr-Nd data and geographic characteristics in sand (soil) samples from

245   the local exposed bedrock and long-distance dust transport of arid deserts. The same

246   Sr-Nd measurement methods were used in these snow samples (Xu et al., 2012; Du et

247   al., 2015, 2019a; Dong et al., 2018, Wei et al., 2019, 2021), and a similar

248   measurement method was used in those sand or surface dust samples (Chen et al.,

249   2007; Nagatsuka et al., 2010). The data results seem to remain fully consistent with

250   these references.

251   The sorting criteria for determining PSAs based on mountains and glaciers

252   distribution, geographic features and isotopic values (snow or ice from the Third Pole

253   glaciers, sand (soil) from local and arid deserts), six isotopic sub-regions across the

254   entire Third Pole were divided as follows (Fig. 2):

255   Region I: Samples from glaciers located in the Altai Mountains include snow

256 samples from Musidao glacier and Altay, and sand samples from the Gurbantunggut

257 Desert, with $\varepsilon_{Nd}(0)$ values from -6.6 to -1.2 and $^{87}Sr/^{86}Sr$ values ranging from

258 0.705483 to 0.71480. The highest $\varepsilon_{Nd}(0)$ values were observed in this region (Chen et

259 al., 2007; Xu et al., 2012; Du et al., 2019a).

260   Region II: Samples from the glaciers on the northern margin of the TP include

261 snow samples from the Tianshan Mountains (Tianshan No. 1 glacier and Miaoergou

262 ice cap) and Kunlun Mountains (Muztagata), as well as sand samples from the

263 Taklimakan Desert, with $\varepsilon_{Nd}(0)$ values from -11.8 to -6.9 and $^{87}Sr/^{86}Sr$ values from

264 0.70842 to 0.728641 (Chen et al., 2007; Nagatsuka et al., 2010; Du et al., 2015; Xu et

265 al., 2012; Wei et al., 2019).

266   Region III: The Sr-Nd isotopic characteristics of the glaciers and sand/soil in the

267 interior of the TP include $\varepsilon_{Nd}(0)$ values ranging from -10.5 to -8.6 and $^{87}Sr/^{86}Sr$ values

268 from 0.713192 to 0.721786 (Xu et al., 2012; Du et al., 2019a; Wei et al., 2021).

269   Region IV: The Sr-Nd isotope data from snow and sand (soil) samples from

270 glaciers in the Himalayan Mountains (East Rongbuk, Jiemayangzong and Yala)

271 include $\varepsilon_{Nd}(0)$ values ranging from -28.1 to -10.5 and $^{87}Sr/^{86}Sr$ values ranging from

272 0.724542 to 0.757407 (Xu et al., 2012; Wei et al., 2021).

273   Region V: Samples from the glaciers in the Qilian Mountains include snow

274 samples from the Qilian Mountains and sand (soil and loess) samples from the Hexi

275 Corridor, with $\varepsilon_{Nd}(0)$ values from -15.7 to -7.0 and $^{87}Sr/^{86}Sr$ values from 0.712349 to

276 0.73211 (Wei et al., 2017; Dong et al., 2018). The $\varepsilon_{Nd}(0)$ values have an increasing

277 trend along the Hexi Corridor from west to east: -15.7–-12.9 for Laohugou No. 12

278 glacier (local soil: -13.6), -13.7–-8.58 for Qiyi, -13.8–-13.6 for Shiyi glacier (local

279 soil: -13.8–-13.6), -12.1–-12.0 for Dabanshan snowpack, and -10.9–-7.0 for

280 Lenglongling glacier (Fig. 2, Dong et al., 2018). It is very clear that, based on local

soil data, regional dust makes a significant contribution to these glaciers.

Region VI: Samples from the glaciers in the eastern TP include snow and soil samples from the Hengduan Mountains, with $\varepsilon_{Nd}(0)$ values from -17.1 to -10.1 and $^{87}Sr/^{86}Sr$ values from 0.717145 to 0.735863 (Xu et al., 2012; Dong et al., 2018).

There is an increasing $^{87}Sr/^{86}Sr$ trend from north (region I) to south (region V), and there is a decreasing $\varepsilon_{Nd}(0)$ trend from north (region I) to south (region V). The maximum $^{87}Sr/^{86}Sr$ ratios and minimum $\varepsilon_{Nd}(0)$ values were observed in region V (Fig. 3). The Sr-Nd data in the Third Pole have relatively narrow ranges with distinct features, while the largest uncertainty was observed from Region IV (Fig. 3).
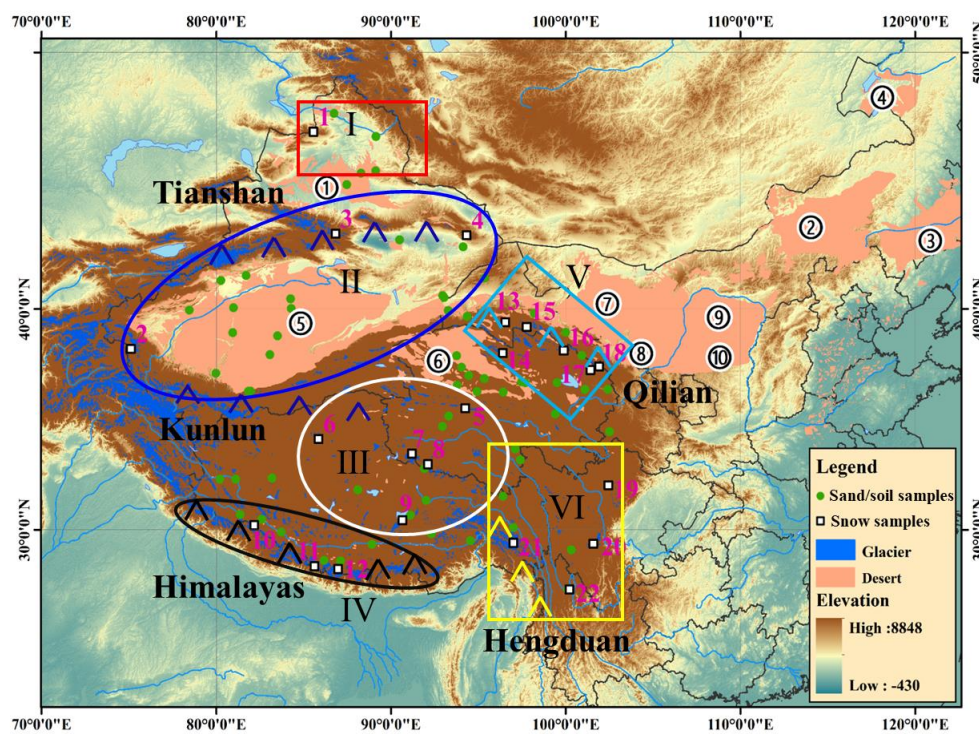
Fig. 2. The glacier and desert distributions in western China (the different coloured oval and rectangular shapes represent six sub-regions (PSAs and glaciers) (Tianshan, Kunlun, Qilian, Himalayas and Hengduan Mountains) in the Third Pole; pink numbers and white rectangles represent 22 glaciers (snow samples were collected

, and green solid circles represent sand/soil samples

(this figure was created with ArcGIS).
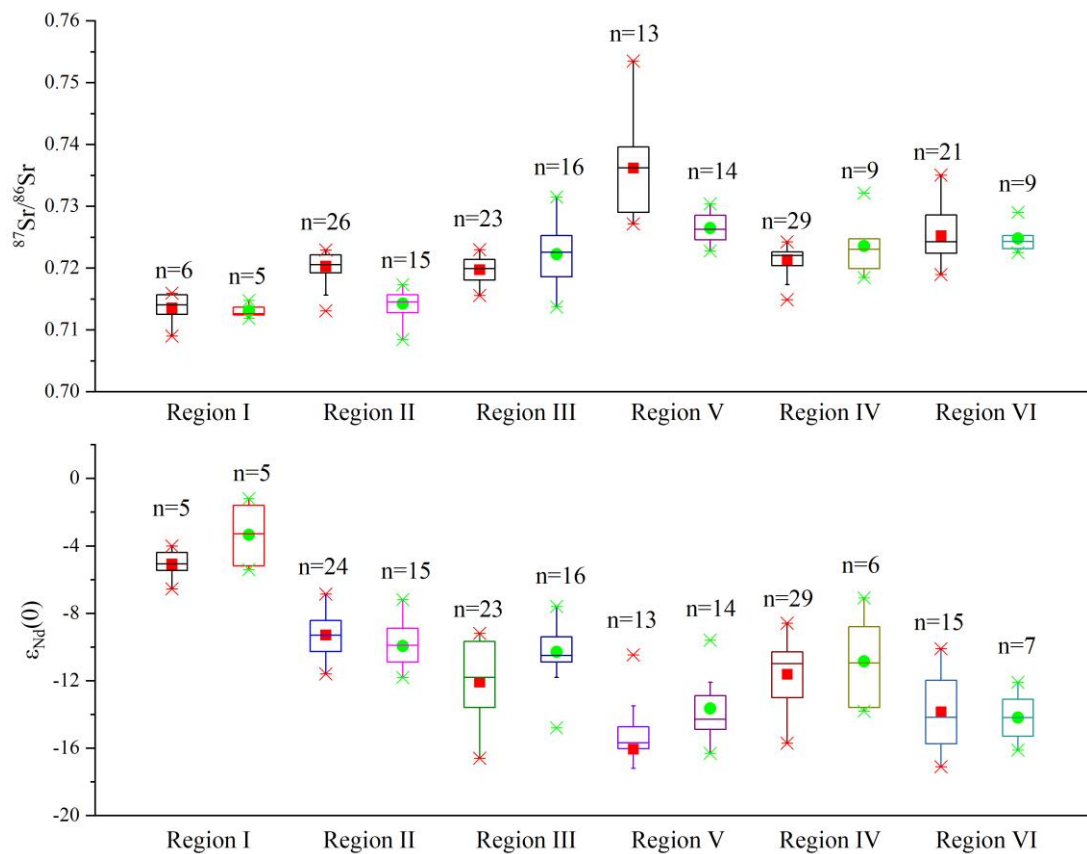
Fig. 3. Box plot for the Sr-Nd isotope signatures of third pole PSAs and snow samples.

Samples are located in each PSA region based on the data from Table 2 (the number

of samples for each sub-region are presented (n>5)). The horizontal line within the

box is the median, and the squares are the mean Sr-Nd values (red rectangles for sand

or soil samples and green solid cycles for snow samples). The interquartile range is

represented by the lower and upper boundaries of the boxes, and whiskers indicate

308 confidence intervals of 1.5 times the interquartile range.

309 **3.2. Sr-Nd data from the Arctic**

310 Considerable Sr-Nd data have been obtained from modern snow/ice samples from the

311 Arctic and surface (including sea ice-transported sediments) sediment from the AO,

312 which covers the entire Arctic and represents the characteristics of sinks (Fig. 4). The

313 data points are presented in Table 3. Sr-Nd data from arid deserts (East Asian and

314 Saharan deserts) have been compiled in previous datasets (Blanchet et al., 2019;

315 Robinson et al., 2021), and these data are useful for tracing terrigenous material

316 transport in the Arctic. For user-friendly selection of the Sr-Nd data according to the

317 modern environment characteristics and the geographical location, Sr-Nd data from

318 the deep ice core are not included in Fig. 5. We compared the Sr-Nd data from the

319 surface snow (sink) and marine sediment (sink or source) samples in the Arctic (Figs.

320 5 and 6). Based on the isotopic signals of these samples, geologic units, adjacent seas

321 and drainage basins of the main river systems in the Arctic, the Sr-Nd patterns can be

322 divided into 12 sub-regions according to Maccali et al. (2018).
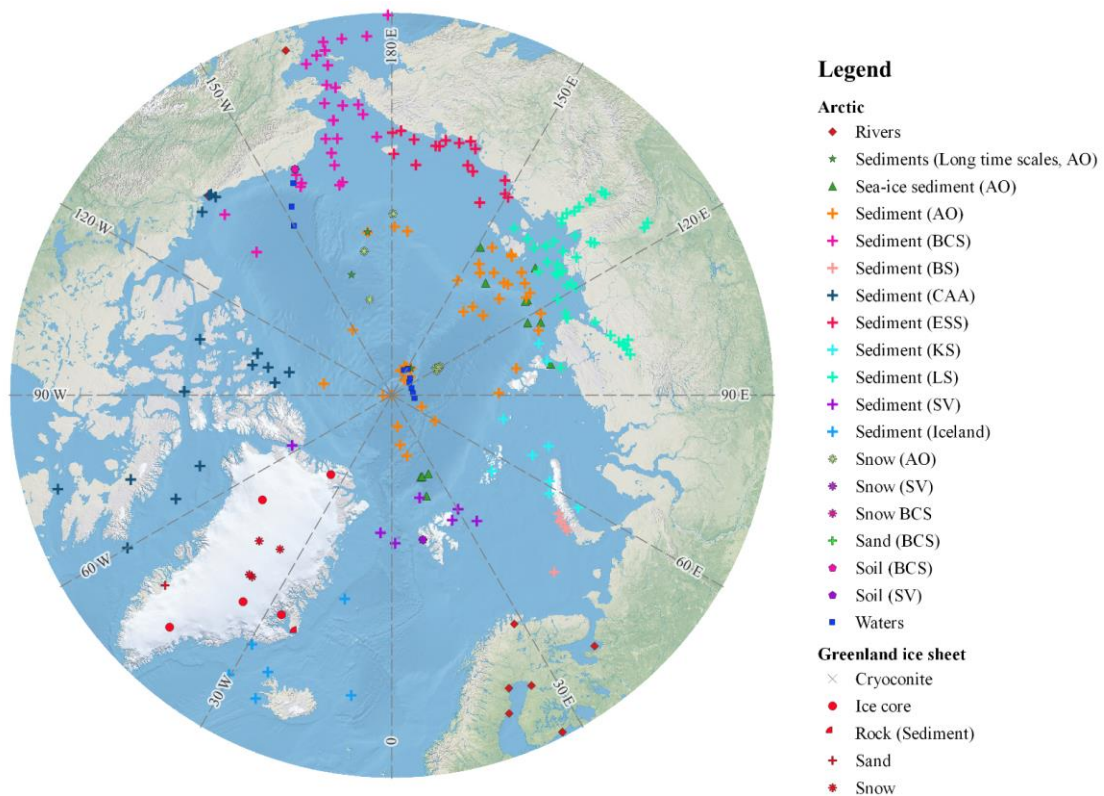
323

324 Fig. 4. Sampling distribution sites in the Arctic. The types of samples are denoted

325 with different shapes and colours (Table 3). (AO: Arctic Ocean; BCS: Bering-Chukchi

326 Sea; BS: Barents Sea; CAA: Canadian Arctic Archipelago; ESS: East Siberian Sea;

327 KS: Kara Sea; LS: Laptev Sea; SV: Svalbard) (this figure was created with ArcGIS).

328 **3.2.1 Sr-Nd data from snow/ice and sand samples of the Greenland ice sheet**

329 Sr-Nd data from the East Greenland Ice Core Project (EGRIP) and the North

330 GRIP (NGRIP) were measured via snowpits. Sr-Nd data were also measured in GRIP,

331 GISP2 and NEEM ice cores, and Renland, Site A, Hans Tausen and Dye 3 shallow ice

332 cores. Sr-Nd data exhibit large differences in these samples (Fig. 5). The Sr-Nd data

333 indicated that the dust sources were variable and showed complicated dust sources in

334 the same location for NGRIP snow (Bory et al., 2002; Bory et al., 2003b). As much

335 more Sr-Nd data from the sand, soil, cryoconite, moraine, and englacial dust samples

336 in the periphery of the GrIS were recently measured (Nagatsuka et al., 2016), ^{87}Sr/^{86}Sr

337 values are high and the $\varepsilon_{Nd}(0)$ values are the least radiogenic in these samples (Table

3). Compared with Sr data in NGRIP and EGRIP snowpits (Bory et al., 2002; Bory et al., 2003b), much larger variations were observed for $^{87}Sr/^{86}Sr$ in the EGRIP snowpit, and relatively lower $^{87}Sr/^{86}Sr$ values were observed in the NGRIP snowpit. The $\varepsilon_{Nd}(0)$ values in the interior of the GrIS are relatively consistent, while the large differences are observed at the periphery of the GrIS. Therefore, although the Sr-Nd isotope ratios indicated that Asian deserts might be the main dust source for the GrIS, the ice-free region around the GrIS might be another source for the interior GrIS. Sr-Nd data in sediment samples collected from the Scoresby Sund region by Simonsen et al. (2019) are as follows: the $^{87}Sr/^{86}Sr$ ratios range from 0.709689 to 0.736137, and the $\varepsilon_{Nd}(0)$ values range from -15.7 to -10.1. Combining Sr-Nd values in snow (Renland, Site A, Hans Tausen and Dye 3) and Dye 3 shallow ice core samples, as proposed by Lupker et al. (2010), the local dust sources may contribute some of the dust to the inland regions and the Sahara is also the most likely additional PSA. Thes local dust for the free ice of the GrIS may have been neglected in previous studies.
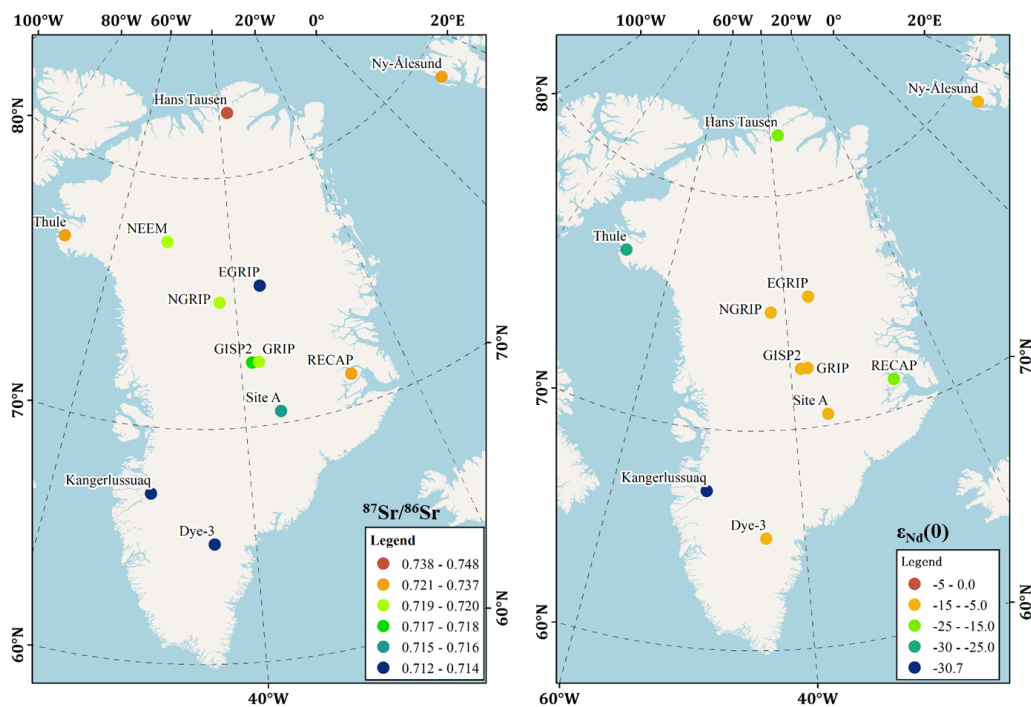
The mainstream view of the provenance of dust in inland Greenland deep ice cores (GISP2 and GRIP) is that the dust is from the eastern Asian deserts (the Gobi and Taklimakan Deserts) based on the best Sr-Nd data matches during the last glacial period (Biscaye et al., 1997; Svensson et al., 2000; Újvári et al., 2015). High-resolution Sr isotope data from the Greenland NEEM ice core suggested that there was a significant Saharan dust influence in Greenland during the last glacial period (Han et al., 2018). The Sr-Nd data (>5 μm) in Holocene RECAP ice core samples are attributed to proximal dust sources; however, the resolution of the data is approximately one thousand years (Simonsen et al., 2019). However, the Sr-Nd data in Greenland deep ice core samples (Biscaye et al., 1997; Svensson et al., 2000), which have low resolutions and represent multiyear averages with no seasonal or interannual variations (60 to 200 cm or 30-150 years), need to be considered when using some data.

3.2.2 Sr-Nd data from snow and sediment samples in the Arctic Ocean

Surface aeolian dust from mid- or high-latitude continental weathering and arid deserts may be the most important dust contributor to snow and ice cores. The $^{87}Sr/^{86}Sr$ values are higher and $\varepsilon_{Nd}(0)$ values are lower in snow and sand samples from Ny-Ålesund, Svalbard (SV) (not including data from Iceland in Fig. 6). The Sr-Nd data in snow samples from sea ice were measured in bulk, and four of these samples were collected near the North Pole in the western AO by MOSAIC (October 2020) in this study (Figs. 4 and 6). The $\varepsilon_{Nd}(0)$ data have much more negative $\varepsilon_{Nd}(0)$ values (-20.8 to -19.6), which cannot be explained by low latitude potential dust sources. As shown in Fig. 6, the lowest ε_{Nd} values were observed along the ice-free periphery of

378 the GrIS and SV; therefore, these ice-free regions are potential dust sources for natural

379 dust in the AO.
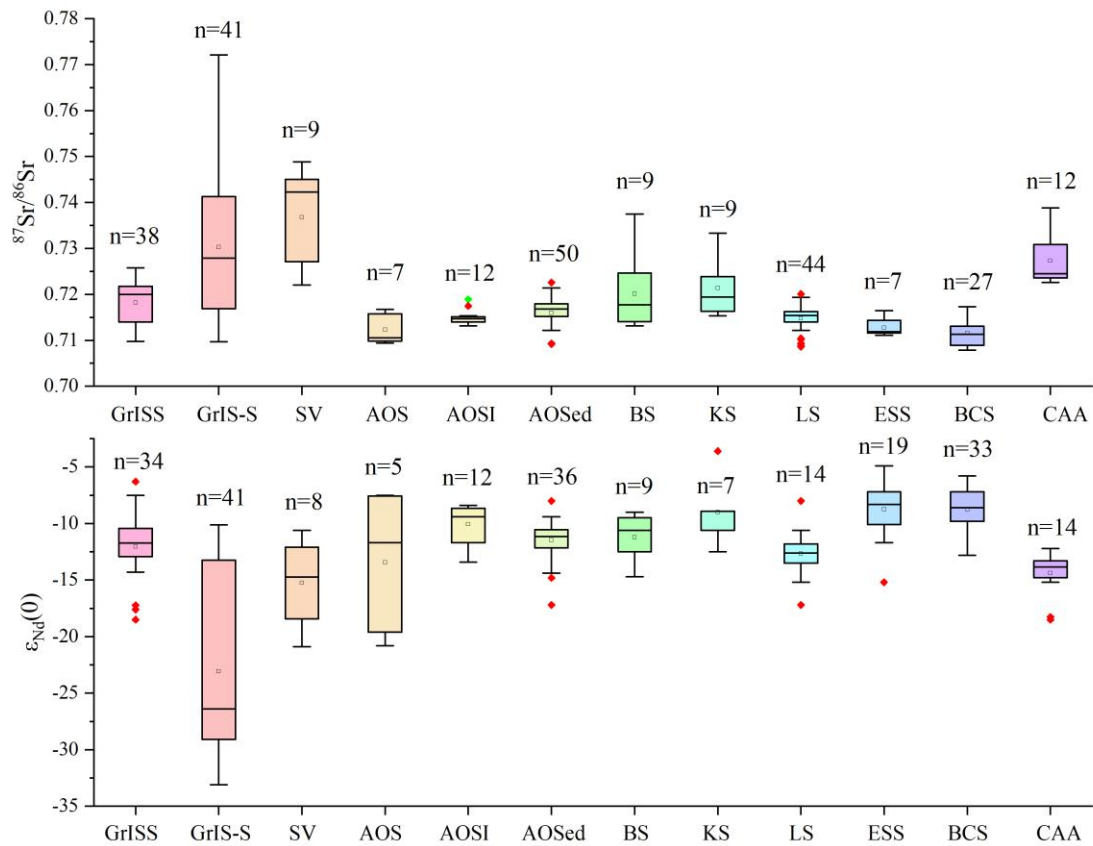
380

381 Fig. 6. Box plot for the Sr-Nd isotopic signatures of the Arctic, including the 12

382 sub-region samples of snow, sand, soil, sediment from sea ice and sediment cores in

383 dataset (the number of samples for each sub-region are presented (n>5)). (GrIS:

384 Greenland ice sheet (snow samples); GrIS-S: Greenland ice sheet (sand); SV:

385 Svalbard (snow and sand); AOS: Arctic Ocean (sediment); AOSI: Arctic Ocean (sea

386 ice sediment)).

387 The terrigenous material from the Arctic margin sea, including BS, KS, LS, ESS,

388 BCS and CAA, was transported and deposited into the AO, which may be the primary

389 material source for marine sediment. The Sr-Nd data from Arctic surface sediments

390 were based on the literature (Fig. 6), and most samples were sieved at < 45 or 63 μm

391 for bulk. These samples were chosen at the surface or 0-10 cm from the top to better

3.3. Information on Sr-Nd data from the SH and Antarctic ice sheet

By integrating the literature and adding data with new evidence, dust provenances of low-elevation areas on the periphery of the AIS in the Holocene (including modern) were discussed. The dataset provides a comprehensive overview of the state of knowledge of dust sources and sinks in different sectors of the AIS and PSAs in the SH. The location Sr-Nd datasets from different sectors of Antarctica and AIS are presented in Fig. 7. Sr-Nd data from Antarctica are not evenly distributed, and more data were measured in western Antarctica and the Ross Sea. Sr-Nd data in PSAs from the SH (Australia, southern South America (hereafter SSA) and southern Africa (SA)) clearly showed characteristics in these regions and provided insight for tracing dust source–sink paths. For example, $^{87}Sr/^{86}Sr$ ratios in Australian dust samples range from 0.709 to 0.732, and $\varepsilon_{Nd}(0)$ values are between -15 and -3 (Revel-Rolland et al., 2006). Sr-Nd data in Patagonia (39–52 °S) of SSA with more radiogenic Nd (-1–1 for $\varepsilon_{Nd}(0)$) (Gaiero, 2007). The aeolian dust from Argentina and Chile is confined to the ranges of $0.7045< {}^{87}Sr/^{86}Sr <0.7130$ and $-5 <\varepsilon_{Nd}(0) <3$ (Delmonte et al., 2003). The

417   ^{87}Sr/^{86}Sr ratios in the sand samples from SA varied between 0.712348 and 0.74716,

418 and the $\varepsilon_{Nd}(0)$ ratios varied between -24.5 and -8.4 (Delmonte et al., 2003; Gili et al.,

419 2021). These Sr-Nd data can very clearly distinguish geographic subgroups for PSAs

420 in SH.
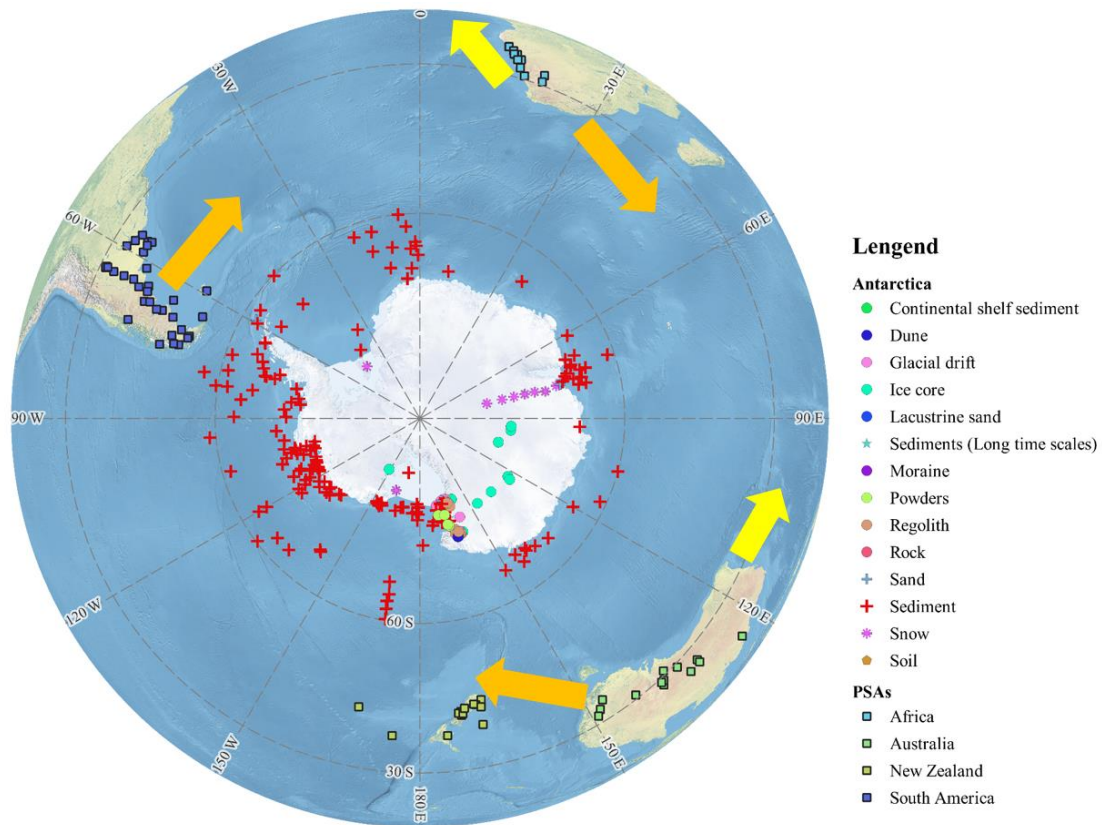
421

422 Fig. 7. The locations of the samples were marked in this database for Sr-Nd isotope

423 ratios from Antarctica and PSAs. The dust transport paths are marked with yellow

424 arrows based on previous studies (Gaiero, 2007; Shao et al., 2010; Gili et al., 2021)

425 (this figure was created with ArcGIS).

426 **3.3.1 Sr-Nd data of sediment in Antarctica**

427   Sr-Nd data for the marine sediment (near-core-top samples) from the

428 Circum-Antarctica, terrigenous materials (aeolian dust, glacial drift and dust in ice

429 core) from the AIS are presented in Fig. 8. The ages of these samples were limited to

430 the Holocene. We compared these data with PSA samples from SH. At some sites, if

431 the samples are >2, we obtained the average Sr-Nd values in this map. For example,

for the Pacific sector (146.78 °E-67.27 °W), $^{87}Sr/^{86}Sr$ values ranged from 0.705281 to 0.725643; $^{87}Sr/^{86}Sr$ values ranged from 0.710616 to 0.738862 for the Indian Ocean sector (20.00 °E-146.78 °E); $^{87}Sr/^{86}Sr$ values ranged from 0.715989 to 0.741609 for the Atlantic sector (67.27 °W-20.00 °E) (Hemming et al., 2007). Viewed from Fig. 8, Sr and Nd contours were determined by inverse distance weighted interpolation, and the numbers of data were >2 in some sites, the averages of surface samples were obtained, the patterns of the two isotopic compositions are consistent in all AIS. Although $^{87}Sr/^{86}Sr$ values differ between sediments from the Circum-Antarctica and sand of PSAs (Australia, SSA and SA), the $^{87}Sr/^{86}Sr$ and $\varepsilon_{Nd}(0)$ patterns from the Pacific sector and Indian Ocean sector are relatively consistent with SSA and SA, which can partly explain the aeolian dust contributing to the entire SO. It seems to be abnormal Sr-Nd values that were found in the Ross Sea and Amundsen Sea, which may have contributed to many more sample numbers in the two regions.
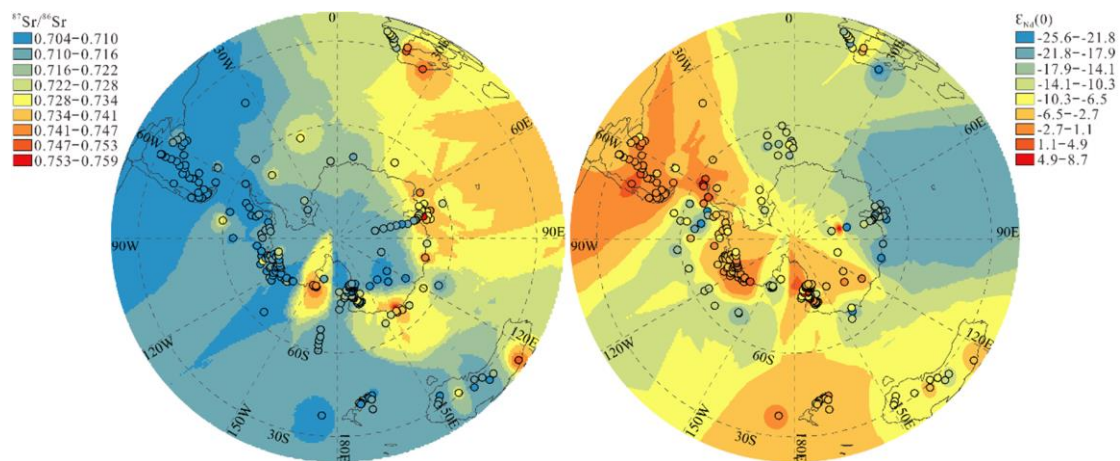
Fig. 8. Sr versus Nd isotopic compositions for Holocene samples (black circles) at the AIS and its periphery in ice-free areas, and aeolian dust samples (surface samples with no accurate ages) from PSAs in Australia, southern Africa and South America defined by colours, which were determined by inverse distance weighted interpolation using ArcGIS.

3.3.2 Sr-Nd data on the periphery and interior of the Antarctic ice sheet

452   New Sr-Nd data from coastal and low-elevation sites were measured in ice-free

453   areas near the Filchner–Ronne Ice Shelf, Ross Ice Shelf and Amery Ice Shelf (Fig. 7).

454   Sr-Nd isotope compositions of four sand samples from southern King George Island

455   (South Shetland Islands) in West Antarctica, with less radiogenic $^{87}Sr/^{86}Sr$ values

456   ranging from ~0.703907 to ~0.704157 and relatively higher $\varepsilon_{Nd}(0)$ values ranging

457   from 4.6 to 6.4. The $^{87}Sr/^{86}Sr$ ratios ranged from 0.71135 to 0.72377, and the $\varepsilon_{Nd}(0)$

458   composition ranged from -13.3 to -9.6 from ice-free areas of Inexpressible Island in

459   the Ross Sea, West Antarctica. Based on the Sr-Nd data on our own and the literature

460   (Table 3), we can observe the highest $\varepsilon_{Nd}(0)$ value of >-5.0 in McMurdo and King

461   George Island. The large variations in $^{87}Sr/^{86}Sr$ values and moderate $\varepsilon_{Nd}(0)$ values for

462   Victoria Land and Ross Sea (including Inexpressible Island). The high $^{87}Sr/^{86}Sr$ ratios

463   and low $\varepsilon_{Nd}(0)$ values for the Amery Ice Shelf have the lowest $\varepsilon_{Nd}(0)$ values of <-15.

464   These sub-regions are very close to $\varepsilon_{Nd}(0)$ data from the different sectors of

465   circumpolar sediments (Roy et al., 2007). Therefore, the dataset will be useful for

466   tracing the dust sources or sinks in SO or AIS.

467   However, among these regions, Sr-Nd data have significant differences in some

468   of the endmembers, which are similar, and care must be taken when directly

469   comparing these data to precisely explain the observed isotopic compositions in ice

470   core records. For example, there is overlap of the Sr and Nd isotopic compositions of

471   King George Island, SSA (Patagonia) and McMurdo dry valleys. Sr-Nd data from

472   Inexpressible Island also overlap with the other endmembers (SA, New South Wale

473   and Prydz Bay). Therefore, dust from low-latitude regions (New South Wale and SA)

474   cannot be excluded from East Antarctica (Du et al., 2018; Gili et al., 2021). Another

475   example is the characteristics of snow layers at the Berkner Island ice sheet in western

476   Antarctica. These data can be partly explained by the surface sediment samples from

the Weddell Sea sector, with $\varepsilon_{Nd}(0)$ values ranging from -10 to -8 (Hemming et al., 2007). Therefore, the dataset from the SH and AIS demonstrates that multiple mixed sources can be inferred for Antarctic surface snow samples. However, among the data from the entire AIS, Sr-Nd isotopic components were measured in only 29 snow samples, and there is an urgent need to collect more data in the future.

Information on Sr-Nd data in Antarctic ice cores during the Holocene and glacial-interglacial times is presented by integrating the literature (Du et al., 2022). To obtain enough dust particles, the different age interval samples were merged. For example, each sample represents approximately 40-160 years for the Vostok ice core, which is a few thousand years to obtain a single large-volume sample (Delmonte et al., 2008). Alternatively, several ice core sections from different depths were integrated to obtain a few large samples for the Sr and Nd isotope analyses of the Talos Dome ice core (Delmonte et al., 2010b). A relatively high resolution (spanning between ~ 3 and ~ 30 yrs.) was used in the Taylor Dome ice core (Aarons et al., 2016). Sr-Nd data in the Antarctica deep ice core mainly focus on the coastal and inland areas of the EAIS. As previously mentioned, the dust source is similar to that of the modern samples in the Dome C and Vostok ice cores during the Holocene and interglacial periods, which can be explained by an SSA provenance; an additional hypothesis explains the isotopic signature of Holocene dust in central East Antarctica (Delmonte et al., 2008, Delmonte et al., 2019). Sr-Nd data in the Talos Dome, Taylor Dome and Taylor Glacier ice cores during the Holocene point towards a local dust provenance (Delmonte et al., 2019; Aarons et al., 2016, 2017). Therefore, the Sr and Nd data from East Antarctica ice cores during the Holocene and interglacial periods indicate a well-mixed atmospheric background involving a mixture of two or more sources in the SH (Fig. 8). The study demonstrated that SA emerges as the second most

502 important dust source to East Antarctica during interglacial periods (Gili et al., 2021).

503 However, the glacial stage (stage 4: ~ 60 ka and stage 6: ~ 160 ka) samples in the

504 Vostok ice core span a very narrow range of Sr compositions ($0.708219 < ^{87}Sr/^{86}Sr <$

505 0.708452) and Nd compositions ($1.1 < \varepsilon_{Nd}(0) < 5.0$), which can also be explained by

506 the Sr-Nd data in sand samples from southern King George Island ($^{87}Sr/^{86}Sr$ values

507 ranging from ~0.703907 to ~0.704157 and $\varepsilon_{Nd}(0)$ values ranging from 4.6 to 6.4).

508 The $^{87}Sr/^{86}Sr$ and $\varepsilon_{Nd}(0)$ isotopic compositions of dust in the Taylor Glacier ice core

509 samples during the last glacial period indicated that dust may originate from SSA and

510 from potential local source areas in the Ross Sea Sector (Delmonte et al., 2010b;

511 Aarons et al., 2016; Aarons et al., 2017). Therefore, these data suggest that the

512 glacial-period dust in East Antarctic ice cores also contributes from local

513 contributions. However, almost no Sr-Nd data were obtained from West Antarctic

514 deep ice cores, which limits our understanding of the dust transport in the spatial and

515 temporal distribution of the entire AIS. More importantly, the ages of Sr-Nd data in

516 surface aeolian dust from the AIS and PSAs from SH are unknown, which is limited

517 to accurate dust source or sink tracing.

518 **4.Data availability**

519 All datasets and the associated metadata table presented in this study are

520 available through a Big Earth Data Platform for Three Poles. The dataset can be

521 downloaded from https://doi.org/10.11888/Cryos.tpdc.272100) (Du et al., 2022). In

522 this repository, all datasets are provided in Excel spreadsheet format together with

523 metadata files.

524 **5. Conclusions**

525 The maintenance integrated Sr-Nd dataset was presented from the remote three

526 poles, and these data are not easily collected because of the extremely cold and high

altitude environment. The dataset is complicated and includes snow, sand, soil, loess, deposits, sediment and other types. We presented case studies of snow, ice core and sediment are intended to demonstrate the Sr-Nd characteristics in the Third Pole glaciers or Arctic and Antarctica ice sheets. These integrated data can provide a new perspective into present and paleodust sources or sinks from the three poles, more importantly, which clearly emphasizes the following points for potential users of the datasets provided with this paper:

1. This Sr-Nd dataset enables us to map the standardized locations in the remote three poles, while the use of sorting criteria related to the sample location, type or resolution permits us to trace the dust sources or sinks based on their isotopic signatures.

2. For the third pole, each sub-region of Sr-Nd data was provided, the integration of these data between sand (soil) and snow samples for six sub-regions allowed us to clearly understand the Sr-Nd data characteristics in the Third Pole. The data will be useful for tracing the local or long-distance transported dust of the source and sink for user.

3. The Sr-Nd characteristics in snow (ice) and sediment samples showed that there are significant differences in different sub-regions for the entire Arctic, which would be useful for tracing dust sources or sinks

4. The new data from Arctic and Antarctic samples emphasized the ice-free regions on the periphery of the ice sheets, which may be important local dust sources. However, in particular, Sr-Nd data overlap with the low-latitude regions in Antarctica, the paucity of data in Antarctica is serious and future studies should concentrate on this aspect.

Author contributions. CX, ZD, and SA designed the study, ZD, JY, CX and SA

wrote the manuscript. ZD, LW, NW, SW, YL collected the samples in the field and produced the data. ZD, NW, LW, SW, YL, ZW, and XM performed the analysis. All authors contributed to the final form of the manuscript.

Competing interests. The authors declare that they have no conflicts of interest.

This work was supported by the Strategic Priority Research Program of the Chinese Academy of Sciences (XAD19070103), the National Natural Science Foundation of China (Grant Nos. 42071086 and 41971088), the National Key Research and Development Program of China (2020YFA0608501), the State Key Laboratory of Cryospheric Science (SKLCS-ZZ-2022) and the Youth Innovation Promotion Association, CAS (2020419). EGRIP is organized by the Center of Ice and Climate at the Niels Bohr Institute and US NSF, Office of Polar Programs. It is supported by funding agencies and institutions in Denmark (A. P. Møller Foundation, UCPH), US (US NSF, Office of Polar Programs), Germany (AWI), Japan (NIPR and ArCS), Norway (BFS), Switzerland (SNF), France (IPEV, IGE), and China (CAS). We thank all people involved in snow samples collecting from central Arctic Ocean by the expedition of the Research Vessel Polarstern for their great logistical supports during MOSAiC in 2019–2020. We also thank the Chinese Arctic and Antarctic Administration contributing to the part of MOSAiC.

References:
Aarons, S., Aciego, S., Gabrielli, P., Delmonte, B., Koornneef, J., Wegner, A., and Blakowski, M.: The impact of glacier retreat from the Ross Sea on local climate: Characterization of mineral dust in the Taylor Dome ice core, East Antarctica, Earth Planet. Sc. Lett, 444, 34–44, https://doi.org/10.1016/j.epsl.2016.03.035, 2016.
Aarons, S. M., Aciego, S. M., Arendt, C. A., Blakowski, M. A., Steigmeyer, A., Gabrielli, P., SierraHernández, M. R., Beaudon, E., Delmonte, B., Baccolo, G., May, N. W., and Pratt, K. A.: Dust composition changes from Taylor Glacier (East Antarctica) during the last glacial-interglacial transition: A multi-proxy approach, Quat. Sci. Rev, 162, 60-71, https://doi.org/10.1016/j.quascirev.2017.03.011, 2017.
Abbott, A. N., Löhr, S. C., Payne, A., Kumar, H., and Du, J.: Widespread lithogenic control of marine

authigenic neodymium isotope records? Implications for paleoceanographic reconstructions. Geochimica et Cosmochimica Acta, 319, 318-336. https://doi.org/10.1016/j.gca.2021.11.021.

Asahara, Y., Takeuchi, F., Nagashima, K., Harada, N., Yamamoto, K., Oguri, K., Tadai, O.: Provenance of terrigenous detritus of the surface sediments in the Bering and Chukchi Seas as derived from Sr and Nd isotopes: implications for recent climate change in the Arctic regions. Deep Sea Res. Part II 61–64, 155–171. https://doi.org/10.1016/j.dsr2.2011.12.004, 2012.

Bayon, G., German, C.R., Boella, R.M., Milton, J.A., Taylor, R.N., Nesbitt, R.W.: An improved method for extracting marine sediment fractions and its application to Sr and Nd isotopic analysis. Chem. Geol. 187, 179-199. https://doi.org/10.1016/S0009-2541(01)00416-8, 2002.

Bayon, G., Freslon, N., Germain, Y., Bindeman, I.N., Trinquier, A., Barrat, J.A.: A global survey of radiogenic strontium isotopes in river sediments. Chem. Geol. 559, 119958. https://doi.org/10.1016/j.epsl.2022.117490, 2021.

Biscaye, P.E., Grousset, F.E., Revel, M., Van der Gaast, S., Zielinski, G.A., Vaars, A., and Kukla, G.: Asian provenance of glacial dust (stage 2) in the Greenland Ice Sheet Project 2 ice core, Summit, Greenland. J. Geophys. Res.-Oceans, 102, 26765-26781. https://doi.org/10.1029/97JC01249, 1997.

Blakowski, M.A., Aciego, S.M., Delmonte, B., Baroni, C., Salvatore, M.C., Sims, K.W.W.: A Sr–Nd–Hf isotope characterization of dust source areas in Victoria Land and the McMurdo Sound sector of Antarctica. Quat. Sci. Rev. 141, 26–37. https://doi.org/10.1016/j.quascirev.2016.03.023.

Blanchet C L.: A database of marine and terrestrial radiogenic Nd and Sr isotopes for tracing earth-surface processes. Earth Syst. Sci. Data, 11(2):741-759. https://doi.org/10.5194/essd-11-741-2019, 2019.

Bory, J. M., Biscaye, P. E., Svensson, A., and Grousset, F. E.: Seasonal variability in the origin of recent atmospheric mineral dust at NorthGRIP, Greenland. Earth Planet. Sc. Lett, 196(3-4):123-134. https://doi.org/10.1016/S0012-821X(01)00609-4, 2002.

Bory, A.M., Biscaye, P.E., Piotrowski, A.M., Steffensen, J.P.: Regional variability of ice core dust composition and provenance in Greenland. Geochem. Geophy. Geosy, 4. https://doi.org/10.1029/2003GC000627, 2003a.

Bory, A.J.M., Biscaye, P.E., Grousset, F.E.: Two distinct seasonal Asian source regions for mineral dust deposited in Greenland (NorthGRIP). Earth Sci. Rev, 30. https://doi.org/10.1029/2002GL016446, 2003b.

Bory, A., Wolff, E., Mulvaney, R., Jagoutz, E., Wegner, A., Ruth, U., and Elderfield, H.: Multiple sources supply eolian mineral dust to the atlantic sector of coastal antarctica: evidence from recent snow layers at the top of Berkner island ice sheet, Earth Planet. Sci. Lett, 291(1-4), 138-148, https://doi:10.1016/j.epsl.2010.01.006, 2010.

Chen, J., Li, G., Yang, J., Rao, W., Lu, H., Balsam, W., Sun, Y., and Ji, J.: Nd and Sr isotopic characteristics of Chinese deserts: implications for the provenances of Asian dust. Geochimica Et Cosmochimica Acta, 71, 3904-3914, https://doi.org/10.1016/j.gca.2007.04.033, 2007.

Delmonte, B., Quaternary variations and origin of continental dust in East Antarctica, PhD Thesis, Universit à degli Studi di Siena / Universit é Joseph Fourier - Grenoble 1, 2003.

Delmonte, B., Andersson, P.S., Hansson, M., Schoberg, H., Petit, J.R., Basile-Doelsch, I., and Maggi, V.: Aeolian dust in East Antarctica (EPICA-Dome C and Vostok): provenance during glacial ages over the last 800 kyr. Geophys. Res. Lett, 35 (7), L07703, https://doi:10.1029/02008GL033382, 2008.

Delmonte, B., Andersson, P.S., Schoberg, H., Hansson, M., Petit, J.R., Delmas, R., Gaiero, D.M., Maggi, V., and Frezzotti, M.: Geographic provenance of Aeolian dust in East Antarctica during

Pleistocene glaciations: preliminary results from Talos Dome and comparison with East Antarctic and new Andean ice core data. Quat. Sci. Rev, 29, 256–264, https://doi.org/10.1016/j.quascirev.2009.05.010, 2010a.

Delmonte, B., Baroni, C., Andersson, P.S., Schöberg, H., Hansson, M., Aciego, S., Petit, J.-R., Albani, S., Mazzola, C., Maggi, V., and Frezzotti, M.: Aeolian dust in the Talos Dome ice core (East Antarctica, Pacific/Ross Sea sector): Victoria Land versus remote sources over the last two climate cycles. J. Quat. Sci, 25 (8), 1327–1337, https://doi.org/10.1002/jqs.1418, 2010b.

Delmonte, B., Baroni, C., Andersson, P. S., Narcisi, B., Salvatore, M. C., Petit, J. R., Scarchilli, C., Frezzotti, M., Albani, S., and Maggi, V.: Modern and Holocene aeolian dust variability from Talos Dome (Northern Victoria Land) to the interior of the Antarctic ice sheet, Quaternary Sci. Rev, 64, 76–89, doi:10.1016/j.quascirev.2012.11.033, 2013.

Delmonte, B., Paleari, C. I., Andò, S., Garzanti, E., Andersson, P. S., Petit, J. R., Crosta, X., Narcisi, B., Baroni, C., Salvatore, M., Baccolo, G., and Maggi.: Causes of dust size variability in central East Antarctica (Dome B): Atmospheric transport from expanded South American sources during Marine Isotope Stage 2. Quaternary Sci. Rev, 168, 55–68, https://doi.org/10.1016/j.quascirev.2017.05.009, 2017.

Delmonte, B., Winton, H., Baroni, M., Baccolo, G., Hansson, M., Andersson, P., Baroni, C., Salvatore, M., Lanci, L., and Maggi, V.: Holocene dust in East Antarctica: provenance and variability in time and space. Holocene, 30 (4), 546-558, https://doi.org/10.1177/0959683619875188, 2019.

Dong, Z., Shao, Y., Qin, D., Kang, S., Wei, W., Wang, X., and Wang, S.: Hf-Nd-Sr isotopic composition as fingerprint for long-range transported eolian dust deposition in glacier snowpack of eastern Tibetan Plateau. J. Geophys. Res, 123, 7013–7023, https://doi.org/10.1029/2018JD028581, 2018.

Du, Z., Xiao, C., Liu, Y., Wu, G.: Geochemical characteristics of insoluble dust as a tracer in an ice core from Miaoergou Glacier, east Tien Shan. Glob. Planet. Chang, 127, 12-21. http://doi.org/10.1016/j.gloplacha.2015.01.011, 2015.

Du, Z., Xiao, C., Ding, M., and Li, C.: Identification of multiple natural and anthropogenic sources of dust in snow from Zhongshan Station to Dome A, East Antarctica. J. Glaciol, 64: 855–865, https://doi.org/10.1017/jog.2018.72, 2018.

Du, Z., Xiao, C., Wang, Y., Liu, S., and Li, S.: Dust provenance in Pan-third pole modern glacierized regions: What is the regional source?. Environmental Pollution, 250(JUL.): 762-772, https://doi.org/10.1016/j.envpol.2019.04.068, 2019a.

Du, Z., Xiao, C., Dou, T., Li, S., An, H., Liu, S., and Liu K.: Comparison of Sr–Nd–Pb isotopes in insoluble dust between northwestern China and high-latitude regions in the Northern Hemisphere. Atmospheric Environment, 214:116837, https://doi.org/10.1016/j.atmosenv.2019.116837, 2019b.

Gaiero, D.M., Brunet, F., Probst, J.L., Depetris, P.J.: A uniform isotopic and chemical signature of dust exported from Patagonia: rock sources and occurrence in southern environments. Chem. Geol. 238 (1), 107-120, https://doi.org/10.1016/j.chemgeo.2006.11.003, 2007.

Gili, S., Vanderstraeten, A., Chaput, A., King, J., Gaiero, D., Delmonte, B., Vallelonga, P., Formenti, P., Di Biagio, C., Cazanau, M. and Pangui, E.: Southern Africa: The Missing Piece To The Dust Provenance Puzzle of East Antarctica? Communications Earth & Environment, 2021.

Grousset, F. E., Biscaye, P. E., Revel, M.., Petit, J., Pye, K., Joussaume, S., and Jouzel, J.: Antarctic (Dome C) ice-core dust at 18 k.y. B. P.: isotopic constraints on origins, Earth Planet. Sci. Lett, 111, 175–182, https://doi.org/10.1016/0012-821X(92)90177-W, 1992.

Grousset, F. E., Parra, M., Bory, A., Martinez, P., Bertrand, P., Shimmield, G and Ellam, R. M.: Saharan

689   wind regimes traced by the Sr–Nd isotopic composition of subtropical Atlantic sediments: last glacial

690   maximum vs today, Quaternary Sci. Rev, 17, 395–409, https://doi.org/10.1016/S0277-3791(97)00048-6,

691   1998.

692   Han, C., Hur, S. D., Han, Y., Lee, K., Hong, S., Erhardt, T., Fischer, H., Svensson, A., Steffensen, JP.,

693   and Vallelonga, P.: High-resolution isotopic evidence for a potential Saharan provenance of Greenland

694   glacial dust. Sci Rep, 8, 15582, https://doi.org/10.1038/s41598-018-33859-0, 2018.

695   Hemming, S.R., van de Flierdt, T., Goldstein, S.L., Franzese, A.M., Roy, M., Gastineau, G., Landrot, G.:

696   Strontium isotope tracing of terrigenous sediment dispersal in the Antarctic Circumpolar Current:

697   implications for constraining frontal positions. Geochem. Geophys. Geosyst, 8 (6), Q06N13,

698   https://doi:10.1029/2006GC001441, 2007.

699   Jacobsen, S.B., Wasserburg, G.J. (1980) Sm-Nd evolution of chondrites. Earth Planet. Sci. Lett. 50,

700   139-155.

701   Jonell, T.N., Li, Y., Blusztajn, J., Giosan, L., Clift, P.D.: Signal or noise? Isolating grain size effects on

702   Nd and Sr isotope variability in Indus delta sediment provenance. Chem. Geol. 485, 56e73.

703   https://doi.org/10.1016/j.chemgeo.2018.03.036, 2018.

704   Lambert, F., Kug, J. S., Park, R. J., Mahowald, N., Winckler, G., Abe-Ouchi, A., and Lee, J. H.: The

705   role of mineral-dust aerosols in polar temperature amplification, Nat. Clim. Change, 3, 487– 491,

706   https://doi.org/10.1038/nclimate1785, 2013.

707   Li, X., Che, T., Li, X., Wang, L., Duan, A., Shangguan, D., Pan, X., Fang, M., and Bao, Q.: CASEarth

708   Poles: Big data for the Three Poles, B. Am. Meteorol. Soc., 101, E1475–E1491, 2020

709   Lin, Y. C., Feng, J. L.: Aeolian dust contribution to the formation of alpine soils at Amdo (Northern

710   Tibetan Plateau). Geoderma 259, 104e115. https://doi.org/10.1016/j.geoderma.2015.05.012, 2015.

711   Lupker, M., Aciego, S.M., Bourdon,B., Schwander,J., and Stocker, T.F.: Isotopictracing(Sr, Nd, U and

712   Hf) of continental and marine aerosols in an 18th century section of the Dye-3 ice core (Greenland).

713   Earth Planet. Sci. Lett, 295. http://dx.doi.org/10.1016/j.epsl.2010.04.010, 2010.

714   Maccali, J., Hillaire-Marcel, C., Not, C.: Radiogenic isotope (Nd, Pb, Sr) signatures of surface and sea

715   ice-transported sediments from the Arctic Ocean under the present interglacial conditions. Polar

716   Research, 37(1):1442982, 2018. https://doi.org/10.1080/17518369.2018.1442982.

717   Meinhardt, A.K., Pahnke, K., Böning, P., Schnetger, B., Brumsack, H.J.: Climate change and response

718   in bottom water circulation and sediment provenance in the central Arctic Ocean since the last glacial.

719   Chem. Geol. 427, 98–108. http://dx.doi.org/10.1016/j.chemgeo.2016.02.019, 2016.

720   Nagatsuka, N., Takeuchi, N., Nakano, T., Kokado, E., and Li, Z.: Sr, Nd, and Pb stable isotopes of

721   surface dust on Urumqi glacier No.1 in western China. Ann. Glaciol., 51(56), 95–105.

722   https://doi.org/10.3189/172756411795931895, 2010.

723   Nagatsuka, N., Takeuchi, N., Uetake, J., Shimada, R., Onuma, Y., Tanaka, S., and Nakano, T.:

724   Variations in Sr and Nd isotopic ratios of mineral particles in cryoconite in Western Greenland.

725   Frontiers in Earth Science 4, 93, https://doi.org/10.3389/feart.2016.00093, 2016.

726   Rao, W.B., Yang, J.D., Chen, J., Li, G.L.: Sr–Nd isotope geochemistry of eolian dust of the

727   arid-semiarid areas in China: implications for loess provenance and monsoon evolution. Chin. Sci. Bull.

728   51 (12), 1401–1412, 2006. https://doi.org/10.1007/s11434-006-2008-1.

729   Revel, M., Sinko, J. A., Grousset, F. E., and Biscaye, P. E.: Sr and Nd isotopes as tracers of North

730   Atlantic lithic particles: Paleoclimatic implications, Paleoceanography, 11, 95–113,

731   https://doi.org/10.1029/95PA03199, 1996.

732   Revel-Rolland M, De Deckker, P., Delmonte, B., Hesse, P.P., Magee, J.W., Basile-Doelsch, Grousset, F.,

and Bosch, D.: Eastern Australia: A possible source of dust in East Antarctica interglacial ice. Earth Planet. Sc. Lett, 249(1–2): 1–13, https://doi.org/10.1016/j.epsl.2006.06.028, 2006.

Robinson, S., Ivanovic, R., Flierdt, T. Van De, Blanchet, L., Tachikawa, K., Martin, E.E., Falco, C.P.C., Williams, T., Gregoire, L., Plancherel, Y., Jeandel, C., Arsouze, T.: Global continental and marine detrital εNd: an updated compilation for use in understanding marine Nd cycling. Chem. Geol. 567, 120119. https:// doi.org/10.1016/j.chemgeo.2021.120119, 2021.

Roy, M., van de Flierdt, T., Hemming, S. R., and Goldstein, S. L.: ^{40}Ar/^{39}Ar ages of hornblende grains and bulk Sm/Nd isotopes of circum-Antarctic glacio-marine sediments: Implications for sediment provenance in the southern ocean, Chem. Geol., 244, 507–519, https://doi.org/10.1016/j.chemgeo.2007.07.017, 2007.

Shao, Y., Wyrwoll, K.H., Chappell, A., Huang, J., Lin, Z., McTainsh, G.H., Yoon, S.: Dust cycle: an emerging core theme in Earth system science. Aeolian Res. 2 (4), 181–204. https://doi.org/10.1016/j.aeolia.2011.02.001, 2011.

Simonsen, M. F., Baccolo, G., Blunier, T., Borunda, A., Delmonte, B., Frei, R., Goldstein, S., Grinsted, A., Kjær, A.A., Sowers, T., Svensson, A., Vinther, B., Vladimirova, D., Winckler, G., Winstrup, M., and Vallelonga, P.: East Greenland ice core dust record reveals timing of Greenland ice sheet advance and retreat. Nature Communications, 10(1):1-8, https://doi.org/10.1038/s41467-019-12546-2, 2019.

Skiles, S.M., Flanner, M., Cook, J.M. Dumont, M., Painter, T. H.: Radiative forcing by light-absorbing particles in snow. Nature Clim Change 8, 964–971. https://doi.org/10.1038/s41558-018-0296-5, 2018.

Struve, T., Pahnke, K., Lamy, F., Wengler, M., Böning, P., Winckler, G.: A circumpolar dust conveyor in the glacial Southern Ocean. Nature Communications, 11(1), 1–11. https://doi.org/10.1038/s41467-020-18858-y, 2020.

Svensson, A., Biscaye, P.E., Grousset, F.E.: Characterization of late glacial continental dust in the Greenland Ice Core Project ice core. J. Geophys. Res.: Atmosphere, 105, 4637-4656, https://doi.org/10.1029/1999JD901093, 2000.

Tütken, T., Eisenhauer, A., Wiegand, B., Hansen, B.T., 2002. Glacial–interglacial cycles in Sr and Nd isotopic composition of Arctic marine sediments triggered by Svalbard/Barents Sea ice sheet. Marien Geology 182, 351–372. https://doi.org/10.1016/S0025-3227(01)00248-1.

Újvári, G., Stevens, T., Svensson, A., Klötzli, U.S., Manning, C., Németh, T., Kovács, J., Sweeney, M.R., Gocke, M., Wiesenberg, G.L.B., Markovic, S.B., Zech, M.: Two possible source regions for central Greenland last glacial dust. Geophys. Res. Lett. 42, 10,399–310, 408, https://doi.org/10.1002/2015GL066153, 2015.

Walter, H.J., Hegner, E., Diekmann, B., Kuhn, G., van der Loeff, M.M.R.: Provenance and transport of terrigenous sediment in the South Atlantic Ocean and their relations to glacial and interglacial cycles: Nd and Sr isotopic evidence. Geochimica Et Cosmochimica Acta 64 (22), 3813–3827. https://doi.org/10.1016/S0016-7037(00)00476-2, 2000.

Wei, T., Dong, Z., Kang, S., Qin, X., Guo, Z.: Geochemical evidence for sources of surface dust deposited on the Laohugou glacier, Qilian Mountains. Appl. Geochem. 79, 1-8. http://doi.org/10.1016/j.apgeochem.2017.01.024, 2017.

Wei, T., Dong, Z., Kang, S., Rostami, M., Ulbrich, S., and Shao, Y.: Hf-Nd-Sr isotopic fingerprinting for aeolian dust deposited on glaciers in the northeastern Tibetan Plateau region. Glob. Planet. Chang, 177, 69–80, https://doi.org/10.1016/j.gloplacha.2019.03.015, 2019.

Wei, T., Brahney, J., Dong, Z., Kang, S., Zong, C., Guo, J., Yang, Lin., Qin, X.: Hf-Nd-Sr Isotopic Composition of the Tibetan Plateau Dust as a Fingerprint for Regional to Hemispherical Transport.

Environmental Science & Technology, 55(14). https://doi.org/10.1021/acs.est.0c04929, 2021.

Wu, G., Zhang, C., Zhang, X., Tian, L., Yao, T.: Sr and Nd isotopic composition of dust in Dunde ice core, Northern China: implications for source tracing and use as an analogue of long-range transported Asian dust. Earth Planet. Sci. Lett, 299 (3), 409-416. http://doi.org/10.1016/j.epsl.2010.09.021, 2010.

Xie, Y., Liu, L., Kang, C., Chi, Y.: Sr-Nd isotopic characteristics of the Northeast Sandy Land, China and their implications for tracing sources of regional dust. Catena 184, 104303. https://doi.org/10.1016/j.catena.2019.104303, 2020.

Xu, J., Yu, G., Kang, S., Hou, S., Zhang, Q., Ren, J., Qin, D.: Sr-Nd isotope evidence for modern aeolian dust sources in mountain glaciers of western China. J. Glaciol, 58 (211), 859-865. http://doi.org/10.3189/2012JoG12J006, 2012.

Winton, V. H. L., Edwards, R., Delmonte, B., Ellis, A., Andersson, P. S., Bowie, A., Bertler, N. A. N., Neff, P., and Tuohy, A.: Multiple sources of soluble atmospheric iron to Antarctic waters, Global Biogeochem. Cy., 30, 421–437, https://doi.org/10.1002/2015GB005265, 2016.

Table 1. Data distribution locations and sample types for $^{87}Sr/^{86}Sr$ and $\varepsilon_{Nd}(0)$ from 90 references.

Region	Characteristics	Data characteristics	Attribution/ harmonization of coordinates	Attribution sorting of criteria	Number of data points
Third Pole					**485**
Kunnun Mountain (Pamirs)	Peer-reviewed publications	Snow, River Sediment, Moraine	Yes	Yes	39
Tibet Plateau	Peer-reviewed publications and own research articles	Snow, Soil, Sand, River Sediment	Yes	Yes	102
Himalaya Mountain	Peer-reviewed publications	Snow, River Sediment	Yes	Yes	14
Qilian Mountain	Peer-reviewed publications and own research articles	Snow, Ice, River Sediment, Soil, Moraine	Yes	Yes	66
Hengduan Mountain	Peer-reviewed publications	Snow, Soil	Yes	Yes	17
Western Chinese Deserts	Peer-reviewed publications and own research articles	Sand, Dune, Fluvial, Lacustrine, Proluvial	Yes	Yes	219
Chinese Loess Plateau	Peer-reviewed publications and own research articles	Loess	Yes	Yes	21
Others (Qinling and Linxia Basin)	Peer-reviewed publications	River sediment	Yes	Yes	7
Pan-third Pole	Peer-reviewed publications and own research articles	Snow, Ice, Sand, Soil, Loess, Moraine, Lacustrine, Dune	Yes	Yes	250
Arctic					**727**
Greenland ic sheet	Peer-reviewed publications, own research articles and own measurements	Snow, Ice, Cryoconite, Sand, Sediment, Rock	Yes	Yes	186
Svalbard (Atlantic Ocean)	Peer-reviewed publications and own research articles	Snow, Sand, Sediment	Yes	Yes	32

Arctic Ocean	Peer-reviewed publications, own research articles and own measurements	Snow, Sediment, Waters	Yes	Yes	496
Others (Rivers and Alaska)	Peer-reviewed publications and own research articles	Snow, Soil (Sand), River Sediment	Yes	Yes	13
Antarctica					**777**
East Antarctica	Peer-reviewed publications and own research articles	Snow, Ice, Sand, Regolith, Glacial drift, Dune, Moraine, Aeolian deposit, Rock, Sediment	Yes	Yes	298
West Antarctica	Peer-reviewed publications and own measurements	Snow, Ice, Sand, Rock, Sediment	Yes	Yes	44
Southern Ocean	Peer-reviewed publications	Sediment	Yes	Yes	435
PSA in Southern Hemisphere					**181**
South America	Peer-reviewed publications	Loess, Soil, Sediment, Aeolian dust	Yes	Yes	57
Southern Africa	Peer-reviewed publications	Aeolian dust, Loess, Sediment deposit, Aerosol	Yes	Yes	53
Australia	Peer-reviewed publications	Sand, Loess, Dune, Lacustrine, Sediment	Yes	Yes	24
New Zealand	Peer-reviewed publications	Loess, Aeolian deposits	Yes	Yes	16
Others	Peer-reviewed publications	Sediment	Yes	Yes	31
Grain sizes	Peer-reviewed publications	Sand, Loess, Sediment, Rock	Yes	Yes	**206**
Methods	Peer-reviewed publications	Loess, Sand, Cryoconite, Rock, Moraine, Dust, Aerosol, River sediment	Yes	Yes	**209**
Grand total					**2835**

794
795
796
797
798
799
800
801
802
803
804
805
806
807
808

809 Table 2. Snow, sand and soil samples were located in the third pole glaciers and PSAs of dust
810 generation. Headers from left to right: Label: the number of glaciers; Sub-regions; Glacier name; Site
811 name: name of the sampling site where the samples were taken; Longitude and Latitude; sampling
812 location; Sample type: Snow, sand or soil; Elevation: m a.s.l; Isotopic ratios of Sr and $\varepsilon_{Nd}(0)$; Ref.:
813 reference publications. The different colours represent different sub-regions.

Label	Glacier name	Sub-regions	Latitude (° N)	Longitude (° E)	Mountains	Sample type	Elevation (m a.s.l)	$^{86}Sr/^{87}Sr$	$\varepsilon_{Nd}(0)$	Ref
1	Musidao	Region I	47.10	85.55	Altai	Snow	3605	0.713185–0.713571	-6.55--4.80	Xu et al., 2012
2	Muztagata		38.28	75.10	East Pamirs	Snow	6365	0.717187–0.717415	-10.3--8.4	Xu et al., 2012
3	Tienshan No. 1	Region II	43.12	86.82	Tien Shan	Snow, dust	4063	0.719404–0.721728	-10.9--6.9	Nagatsuka et al., 2010; Xu et al., 2012
4	Miaoergou		43.06	94.32	Tiean Shan	Snow, Ice, Cryoconite	3100–4512	0.710284–0.720825	-11.6--7.3	Du et al., 2015; Wei et al., 2019
5	Yuzhufeng Glacier		35.66	94.24	Kulun	Snow	4300–4720	0.714821–0.716757	-16.6--11.8	Wei et al., 2019
6	Zangsegangri		34.27	85.85	Qiangtang	Snow	6226	0.717352–0.718328	-12.9--9.2	Xu et al., 2012
7	Guoqu	Region III	33.58	91.20	Tanggula	Snow	5765	0.717546–0.721786	-10.2--9.5	Xu et al., 2012
8	Dongkemadi		33.10	92.10	Tanggula	Snow	5700	0.713192	-10.5	Xu et al., 2012
9	Zadang		30.47	90.65	Nyainqentangl ha	Snow	5758	0.718285–0.721305	-12.9--11.1	Xu et al., 2012
10	Jiemayangzong		30.22	82.17	Himalaya	Snow	5558	0.72671–0.740694	-14.3--10.5	Xu et al., 2012
11	Yala	Region IV	28.23	85.62	Himalaya	Snow	5190	0.740112	-15.68	Xu et al., 2012
12	East Rongbuk		28.10	86.97	Himalaya	Snow	6525	0.728057–0.757407	-28.1--14.7	Xu et al., 2012
13	Laohugou Glacier No.12		39.43	96.53	Qilian	Snow	4288–5026	0.720448–0.723303	-15.7--9.5	Xu et al., 2012; Wei et al., 2019
14	Dunde ice cap		38.10	96.40	Qilian	Ice	5325	0.715220–0.721874	-11.1--9.9	Wu et al., 2010
15	Qiyi Glacier 1	Region V	39.24	97.76	Qilian	Snow	4500–4750	0.712349–0.722751	-13.7--8.6	Dong et al., 2018
16	Shiyi Glacier		38.21	99.88	Qilian	Snow	3928–4152	0.721032–0.721711	-14.0--13.8	Wei et al., 2019
17	Dabanshan		37.36	101.40	Qilian	Snow	3593–3625	0.723105–0.725015	-12.1--12.0	Wei et al., 2019
18	Lenglongling Glacier		37.52	101.90	Qilian	Snow	3558–3992	0.719084–0.728414	-10.9--7.0	Dong et al., 2018
19	Dagu Glacier		32.12	102.43	Hengduan	snow	3520–3701	0.719216–0.721102	-16.9--12.3	Dong et al., 2018
20	Hailuogou Glacier	Region VI	29.33	101.57	Hengduan	snow	3010–3850	0.722805–0.728326	-17.1--12.0	Dong et al., 2018
21	Demula Glacier		29.37	97.00	Hengduan	Snow	5404	0.729095–0.735863	-17.1--14.2	Xu et al., 2012
22	Baishui Glacier No.1		27.10	100.20	Hengduan	Snow	4338–4747	0.717145–0.719881	-13.8--11.4	Xu et al., 2012; Dong et al., 2018

814
815
816
817
818
819
820
821
822
823
824
825
826
827
828
829
830
831
832
833
834
835

Label	Subregion	Location	Sample type	Time interval	Size fraction	Ref
1	GrISS	East GrIS; North GrIS	snowpit	2017/2018; early-1995	>0.2 μm; <45 or 38 μm	This study; Bory et al., 2002
2	GrIS-S	East GrIS; West GrIS	Cryoconite, Moraine, Englacial dust, Sand, Rock, Sediment	NO	Bulk	This study; Nagatsuka et al., 2016; Simonsen et al., 2019
3	SV	Ny-Ålesund	Snow, Sand, Soil; Sediment	NO	Bulk; <100 μm	Tütken et al., 2002; Maccali et al., 2018; Du et al., 2019b
4	AO	Arctic Ocean	Snow	2016	Bulk	This study; Du et al., 2019b
5	AOSI	Arctic Ocean	Sea ice sediment	NO	<100 μm	Eisenhauer et al., 1999; Tütken et al., 2002
6	AOSed	Arctic Ocean	Sediment	NO	Bulk; <100 μm	Eisenhauer et al., 1999; Tütken et al., 2002; Maccali et al., 2018
7	BS	Arctic Ocean	Sediment	NO	<100 μm	Tütken et al., 2002; Maccali et al., 2018
8	KS	Arctic Ocean	Sediment	NO	<100 μm	Tütken et al., 2002; Maccali et al., 2018
9	LS	Arctic Ocean	Sediment	NO	<100 μm; Bulk	Eisenhauer et al., 1999; Maccali et al., 2018
10	ESS	Arctic Ocean	Sediment	NO	<100 μm	Bazhenova et al., 2017; Maccali et al., 2018
11	BCS	Arctic Ocean	Sediment	NO	<100 μm; Detrital	Asahara et al., 2012; Bazhenova et al., 2017; Maccali et al., 2018; Du et al., 2019b
12	CAA	Arctic Ocean	Sediment	NO	<100 μm	Asahara et al., 2012; Bazhenova et al., 2017; Maccali et al., 2018

839